

Targeting lipid nanoparticles to the blood-brain barrier to ameliorate acute ischemic stroke

Jia Nong,^{1,11} Patrick M. Glassman,^{1,2,11} Vladimir V. Shuvaev,¹ Sahily Reyes-Esteves,³ Helene C. Descamps,⁴ Raisa Y. Kiseleva,¹ Tyler E. Papp,⁵ Mohamad-Gabriel Alameh,⁵ Ying K. Tam,⁶ Barbara L. Mui,⁶ Serena Omo-Lamai,⁷ Marco E. Zamora,¹ Tea Shuvaeva,¹ Evguenia Arguiri,¹ Xijing Gong,⁷ Taylor V. Brysgel,¹ Ai Wen Tan,¹ Ashley G. Woolfork,¹ Aalim Weljie,¹ Christoph A. Thaiss,^{4,8,9} Jacob W. Myerson,¹ Drew Weissman,⁵ Scott E. Kasner,³ Hamideh Parhiz,⁵ Vladimir R. Muzykantov,¹ Jacob S. Brenner,^{1,10} and Oscar A. Marcos-Contreras^{1,3}

¹Department of Systems Pharmacology and Translational Therapeutics, Perelman School of Medicine, University of Pennsylvania, Philadelphia, PA 19104, USA; ²Department of Pharmaceutical Sciences, School of Pharmacy, Temple University, Philadelphia, PA, USA; ³Department of Neurology, Perelman School of Medicine, University of Pennsylvania, Philadelphia, PA, USA; ⁴Department of Microbiology, Perelman School of Medicine, University of Pennsylvania, Philadelphia, PA, USA; ⁵Division of Infectious Diseases, Perelman School of Medicine, University of Pennsylvania, Philadelphia, PA, USA; ⁶Acuitas Therapeutics, Vancouver, British Columbia V6T 1Z3, Canada; ⁷Department of Bioengineering, School of Engineering and Applied Sciences, University of Pennsylvania, Philadelphia, PA, USA; ⁸Institute for Diabetes, Obesity and Metabolism, Perelman School of Medicine, University of Pennsylvania, Philadelphia, PA, USA; ⁹Institute for Immunology, Perelman School of Medicine, University of Pennsylvania, Philadelphia, PA, USA; ¹⁰Division of Pulmonary Allergy, and Critical Care, Department of Medicine, Perelman School of Medicine, University of Pennsylvania, Philadelphia, PA, USA

Effective delivery of mRNA or small molecule drugs to the brain is a significant challenge in developing treatment for acute ischemic stroke (AIS). To address the problem, we have developed targeted nanomedicine to increase drug concentrations in endothelial cells of the blood-brain barrier (BBB) of the injured brain. Inflammation during ischemic stroke causes continuous neuronal death and an increase in the infarct volume. To enable targeted delivery to the inflamed BBB, we conjugated lipid nanocarriers (NCs) with antibodies that bind cell adhesion molecules expressed at the BBB. In the transient middle cerebral artery occlusion mouse model, NCs targeted to vascular cellular adhesion molecule-1 (VCAM) achieved the highest level of brain delivery, nearly two orders of magnitude higher than untargeted ones. VCAM-targeted lipid nanoparticles with luciferase-encoding mRNA and Cre-recombinase showed selective expression in the ischemic brain. Anti-inflammatory drugs administered intravenously after ischemic stroke reduced cerebral infarct volume by 62% (interleukin-10 mRNA) or 35% (dexamethasone) only when they were encapsulated in VCAM-targeted NCs. Thus, VCAM-targeted lipid NCs represent a new platform for strongly concentrating drugs within the compromised BBB of penumbra, thereby ameliorating AIS.

INTRODUCTION

Stroke is the second leading cause of death and the top cause of major disability globally¹; however, there have been no new drug classes approved to treat stroke in more than 25 years. The vast majority (87%) of strokes are classified as acute ischemic stroke (AIS), charac-

terized by occlusion of an artery supplying the brain.² Current treatment of AIS is focused on recanalization and reperfusion of the brain (e.g., removal of the clot), which is performed by enzymatic thrombolysis using tissue-type plasminogen activator (tPA) and derivatives or, since 2015, mechanical thrombectomy.^{3–6} The advent of mechanical thrombectomy has provided great improvement in restoring blood flow to ischemic regions of the brain. However, outcomes of severe AIS (characterized by large vessel occlusion) are poor, with 50%–55% of patients dying or becoming functionally dependent on others.^{2,3,6} To improve outcomes, decades of research have been performed with the goal of salvaging the reperfused or partially reperfused (penumbra) tissue at risk of death. A diverse array of drugs has been tested that focus on the following mechanisms: excitotoxic neuronal

Received 7 August 2023; accepted 5 March 2024;
<https://doi.org/10.1016/j.ymthe.2024.03.004>

¹¹These authors contributed equally

Correspondence: Hamideh Parhiz, Division of Infectious Diseases, Perelman School of Medicine, University of Pennsylvania, Philadelphia, PA, USA.

E-mail: hamideh.parhiz@penncmedicine.upenn.edu

Correspondence: Vladimir R. Muzykantov, Department of Systems Pharmacology and Translational Therapeutics, Perelman School of Medicine, University of Pennsylvania, Philadelphia, PA 19104, USA.

E-mail: muzykant@pennmedicine.upenn.edu

Correspondence: Jacob S. Brenner, Department of Systems Pharmacology and Translational Therapeutics, Perelman School of Medicine, University of Pennsylvania, Philadelphia, PA 19104, USA.

E-mail: jacob.brenner@pennmedicine.upenn.edu

Correspondence: Oscar A. Marcos-Contreras, Department of Systems Pharmacology and Translational Therapeutics, Perelman School of Medicine, University of Pennsylvania, Philadelphia, PA 19104, USA.

E-mail: oscarmar@pennmedicine.upenn.edu

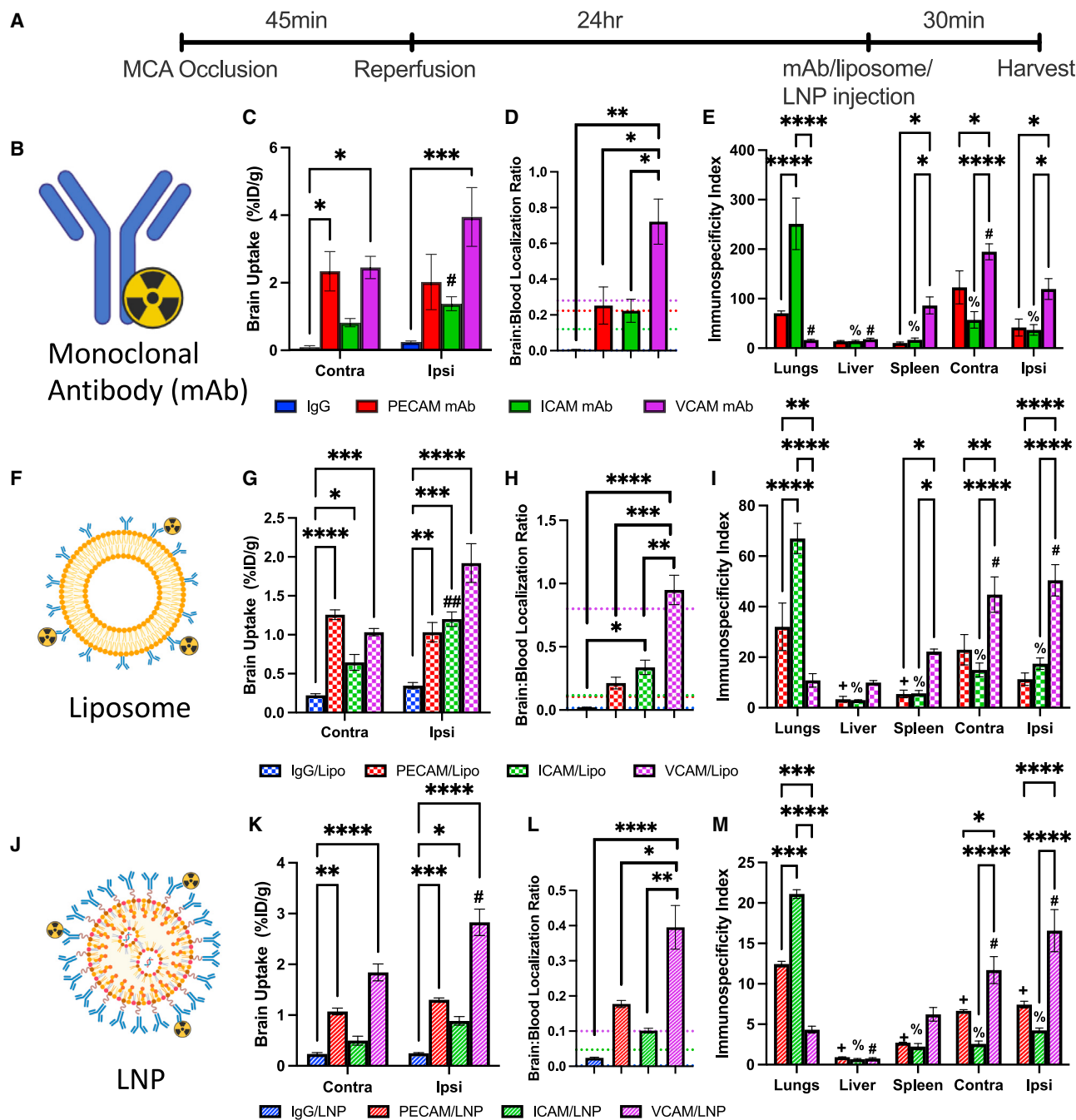


Figure 1. In the tMCAO model of AIS, CAM-targeted antibodies and NPs accumulate in the brain at vastly higher levels

(A) Timeline for all biodistribution experiments. Mice were challenged with ischemia (45 min) and reperfusion, followed by IV injection of ^{125}I -radiolabeled mAbs/liposomes/LNPs or untargeted IgG controls 24 h after injury, and tissue biodistribution was determined 30 min after injection. (B, F, and J) Schematic representation of radiolabeled mAbs, mAb-conjugated liposomes, mAb-conjugated LNPs, respectively. (C, G, and K) All anti-CAM mAbs/liposomes/LNPs had markedly higher brain uptake than control IgG counterpart, with the highest uptake in the ipsilateral (injured) hemisphere being anti-VCAM. Anti-ICAM mAb was the only mAb that showed a statistically significant preference for accumulation in the ipsilateral vs. contralateral hemisphere. * $p < 0.05$, ** $p < 0.01$, * $p < 0.001$, **** $p < 0.0001$ using two-way ANOVA followed by Dunnett's *post hoc* against IgG, # $p < 0.05$, ## $p < 0.01$ using paired t-test comparing contralateral vs. ipsilateral. See also Tables S2–S4. (D, H, and L) The brain-to-blood distribution ratio in ipsilateral tMCAO brain further illustrates the superiority of VCAM-targeted mAbs/liposomes/LNPs. The values observed in naive mice are shown by dashed lines. * $p < 0.05$, ** $p < 0.01$, *** $p < 0.001$, **** $p < 0.0001$ using one-way ANOVA followed by Tukey's *post-hoc* against IgG control. (E) ISI (localization ratio targeted mAb/localization ratio (legend continued on next page)

death, reactive oxygen species for ischemia-reperfusion, neuronal apoptosis, and inflammation. Anti-inflammatory drugs have demonstrated particular promise in preclinical studies, since the inflammatory process starts immediately after the occlusion occurs and promotes neuronal death, and lasts for days to weeks, which aggravates the overall condition in stroke.⁷ Neurovascular inflammatory processes are in part propagated by expression of cellular adhesion molecules (CAMs) by endothelial cells in the penumbra, which help to recruit immune cells to the injured region.^{8–11}

Despite promising results in preclinical studies, all neuroprotectants that progressed to clinical trials have failed in development, with the primary cause of failure being cited as insufficient drug delivery, without causing non-tolerable off-target effects.¹² Several features of AIS make it a particular challenge for drug delivery. First, efficient drug delivery to the brain is notoriously difficult in general due to the nearly impenetrable blood-brain barrier (BBB). Second, poor reperfusion (common prior to mechanical thrombectomy) leads to insufficient blood flow to at-risk brain regions to achieve effective drug accumulation. Third, severe AIS patients are critically ill and often do not tolerate off-target drug effects, resulting in strict limitations on systemic dosing in AIS. Therefore, there is a critical unmet need to improve drug delivery to the brain in AIS, which we hypothesize can be achieved using targeted drug delivery systems.

Nanocarriers (NCs) are particles with diameters of approximately 100 nm that allow the encapsulation and delivery of diverse small molecule drugs and biotherapeutics. Clinical use of NCs originated in the field of oncology with the approval of liposomal doxorubicin (Doxil, Caelyx) in the 1990s. NCs have recently risen to prominence in the form of COVID-19 vaccines (Moderna, BioNTech), which used lipid nanoparticles (LNPs) to encapsulate mRNA, with demonstrated safety and efficacy in a global population (>5 billion doses administered).¹³ Extrahepatic and selective delivery of NCs to tissues, sites of injury, or specific cells is an unmet need and can be achieved by conjugation of affinity ligands on the NC surface. Targeted nanomedicine allows (1) localization and concentration of drugs in the target site and (2) a decrease in off-target toxicities by sparing tissues from drug exposure, thereby increasing the therapeutic index.¹⁴ We hypothesized that targeted NCs would be useful for the treatment of AIS.

It is well-established that inducible cell-surface molecules such as intercellular adhesion molecule-1 (ICAM) and vascular CAM-1 (VCAM) are upregulated in the penumbra in AIS as a result of neuroinflammation.^{15–17} Therefore, we hypothesized that targeting these inducible markers would concentrate our NCs in the injured region of the brain, and provide therapeutic efficacy that free drugs could not achieve by converting the BBB into either a depot (dexamethasone) or a biofactory (interleukin-10 [IL-10]) for anti-inflammatory

therapeutics, thus switching the pro-inflammatory environment into an anti-inflammatory one. In the current study, we used the gold standard animal model of large vessel AIS followed by mechanical thrombectomy (transient middle cerebral artery occlusion [tMCAO]). This model is characterized by occlusion of the MCA with a filament for a pre-defined period of time, followed by filament removal and reperfusion. We have demonstrated that, in this model, (1) VCAM-targeted monoclonal antibodies (mAbs) and NCs (mRNA LNP and liposomes) after intravenous (IV) injection showed superior targeting and specificity to the injured brain compared with ICAM and the constitutively expressed platelet endothelial CAM (PECAM); (2) VCAM-targeted NCs were taken up by endothelial cells and infiltrating leukocytes; (3) VCAM-targeted mRNA LNP encoding for luciferase and Cre-recombinase showed local expression and gene editing in the injured region of the brain following IV dosing of VCAM-targeted LNP; and (4) a 35% decrease in infarct volume after IV dosing of VCAM-targeted, dexamethasone-loaded liposomes; a 62% decrease in infarct volume with a 100% survival following IV administration of VCAM-targeted LNP containing mRNA that encodes very potent anti-inflammatory cytokine IL-10. In summary, these results demonstrated that VCAM targeting is a useful approach to deliver drugs to the inflamed brain vasculature and to improve the efficacy of neuroprotective drugs in a mouse model of AIS.

RESULTS

Targeting the tMCAO brain using mAbs directed against CAMs

Both AIS in humans and tMCAO in mice lead to severe acute inflammation in the penumbra around the core infarct, resulting in upregulation of inducible CAMs (e.g., ICAM and VCAM).^{18,19} Prior studies have shown this increase in CAM expression in tMCAO by measuring mRNA and protein levels in tissue homogenates, or with immunohistology.^{20–22} These studies left an open question: Are the *de novo* expressed ICAM and VCAM proteins accessible to the vessel lumen, allowing adhesion of systemically administered, targeted therapeutics? To assess vascular accessibility of CAMs and to establish their use for targeted drug delivery in tMCAO and AIS, we injected radiolabeled mAbs against PECAM (constitutively expressed), and ICAM and VCAM (inducible) 24 h after reperfusion.²³ Mice were sacrificed and perfused 30 min after the injection to determine the tissue distribution of the mAbs (Figure 1A).

In tMCAO mice, CAM-targeted mAbs (Figure 1B) accumulated in the brain to a significantly higher degree than control immunoglobulin G (IgG), precluding vascular leak as a driver of tissue uptake. Anti-VCAM had the highest brain uptake at $3.95 \pm 0.87\%$ ID/g in the ipsilateral (injured) hemisphere, while IgG control had the lowest uptake ($0.25 \pm 0.03\%$ ID/g). There was no significant difference between the two hemispheres for anti-PECAM mAb ($p = 0.3915$) or anti-VCAM mAb ($p = 0.1722$), but anti-ICAM had a small but statistically

untargeted IgG) of mAbs/liposomes/LNPs in tMCAO mice showed significant lung targeting of ICAM over other organs, non-significant lung targeting of PECAM over other organs, and non-significant higher targeting of VCAM when compare spleen vs. brain. See also Figure S3. $n = 3$. * $p < 0.05$, ** $p < 0.01$, * $p < 0.001$, **** $p < 0.0001$ using two-way ANOVA followed by Tukey's post-hoc. % $p < 0.05$, + $p < 0.05$ using one-way ANOVA followed by Dunnett's *post hoc* against lungs, and # $p < 0.5$ against spleen. Data are presented as mean \pm SEM.

significant preference for the ipsilateral hemisphere ($p = 0.0252$) (Figure 1C). To better understand brain uptake, a more relevant term “localization ratio” or “blood-normalized tissue uptake” is used to determine the brain-to-blood ratio. This helps to demonstrate whether the accumulation is caused by high blood concentrations driving brain uptake, which also produce continued side effects by driving uptake in other tissues. As shown in Figure 1D, in the ipsilateral brain of tMCAO mice, the blood-normalized (localization ratio) brain uptake of anti-VCAM mAb was more than 2-fold higher (0.72 ± 0.13) than anti-PECAM (0.25 ± 0.10) and anti-ICAM mAb (0.22 ± 0.07), and exceeded IgG uptake by more than two orders of magnitude (0.01 ± 0.001). Additionally, compared with naive mice (no tMCAO), only the brain-to-blood uptake of VCAM increased after tMCAO challenge. VCAM mAbs outperformed mAbs for other CAMs in magnitude of brain uptake and in augmentation of uptake by AIS pathology.

We also investigated CAM-targeted mAb uptake in other organs. It is well known that PECAM and ICAM are highly expressed in lungs, VCAM in spleen, and untargeted IgG maintains high concentration in the blood, which is confirmed by the antibody biodistribution (Figure S1A; Table S2). The analysis of the immunospecificity index (ISI; localization ratio targeted mAb/localization ratio untargeted IgG) showed that (1) the ISI of PECAM mAb did not indicate superior lung targeting when comparing among all major organs; (2) the ISI of ICAM mAb remained significantly higher in lungs than other organs, including brain; and (3) the ISI of VCAM mAb in the spleen was significantly higher than in the lungs and liver, but not significantly higher than in contralateral (uninjured) and ipsilateral (injured) brain hemispheres (Figure 1E). These findings are consistent with previous publications with acute brain inflammation.²⁴

VCAM targeting outperforms ICAM and PECAM targeting for mRNA-LNP and liposome delivery to tMCAO brains

Having shown that CAM targeting directs mAbs to the tMCAO brain, we examined CAM targeting with mRNA containing LNPs and liposomes. Compared with mAbs, NCs have vastly different accessibility to membrane epitopes (due to steric hindrance), pharmacokinetics, and binding capacity. We characterized two classes of NCs that are widely used in clinical studies: LNP and liposomes (Figures 1F and 1J). Liposomes have the potential for delivering a wide array of small molecules and protein drugs, including dexamethasone,^{12,25} while LNPs allow delivery of RNA cargoes (e.g., mRNA or small interfering RNA). Our lab has previously published the morphological characterization of liposomes and LNPs using the same formulations.^{24,26–28} The conjugation efficiency of antibodies onto NCs is quantified approximately 85% for liposomes and approximately 95% for LNPs, resulting in approximately 50 antibodies per NC (Figure S2; Table S1). In addition, we have studied the effect of antibody surface density on targeting efficiency in naive and mice challenged by neurovascular inflammation (intra-striatal injection of tumor necrosis factor- α , a high-throughput model) (Figure S3). As there is no significant difference in targeting efficiency when the antibody amount per NCs is greater than 50, we choose 50 antibodies per NC for all subsequent studies in this manuscript to minimize Fc-induced complement activation.²⁹

We evaluated brain uptake of liposomes directed against PECAM, ICAM, and VCAM, compared with untargeted IgG control. CAM targeting significantly enhanced liposome uptake in both hemispheres of tMCAO-challenged brains, compared with untargeted IgG control (Figure 1G). ICAM-targeted liposomes had preferential delivery to the ipsilateral hemisphere in tMCAO (ICAM: $p = 0.0055$). When comparing localization ratio, anti-VCAM liposomes had 50-fold higher ipsilateral accumulation vs. IgG control (0.95 ± 0.12 vs. 0.02 ± 0.004), 4.46-fold higher than anti-PECAM liposomes (0.21 ± 0.05), and 2.82-fold higher than anti-ICAM liposomes (0.34 ± 0.06) (Figure 1H). We observed high pulmonary uptake of anti-PECAM and anti-ICAM liposomes, along with substantial splenic uptake of anti-VCAM liposomes (Figure S1B; Table S3). However, through ISI analysis, we found that anti-VCAM liposomes exhibited superior brain targeting over spleen (Figure 1I).

The CAM-targeted immunoliposomes study design was replicated to assess brain uptake of CAM-targeted LNPs. We evaluated brain uptake of LNPs directed against PECAM, ICAM, and VCAM, compared with untargeted IgG control. Similar to CAM-targeted mAbs and liposomes, within 30 min of injection, anti-VCAM LNPs accumulated in the brain at significantly higher concentrations than untargeted IgG LNPs ($p = 0.0218$). Ipsilateral to contralateral ratios showed a higher selectivity for the ipsilateral part of anti-ICAM and anti-VCAM LNPs compared with anti-PECAM ones (ipsilateral/contralateral ratios: ICAM 1.91 ± 0.43 , VCAM 1.54 ± 0.14 and PECAM 1.22 ± 0.08) (Figure 1K). When comparing the localization ratio of all LNPs in the ipsilateral brain, uptake of anti-VCAM LNP achieved 16.5-fold superiority over untargeted IgG LNPs (0.40 ± 0.1 vs. 0.02 ± 0.002), 2.23-fold superiority over anti-PECAM LNPs (0.18 ± 0.01), and 3.91-fold superiority over anti-ICAM LNPs (0.10 ± 0.01) (Figure 1L). As expected, anti-PECAM and anti-ICAM LNPs also accumulated in the lungs and the absolute delivery to the pulmonary vasculature of these formulations greatly exceeded that in the brain, while anti-VCAM LNPs minimally accumulated in the lungs and were largely taken up in the spleen (Figure S1C; Table S4). However, while the trend of ISI remained unchanged for anti-PECAM and anti-ICAM LNP, it was evident that anti-VCAM LNP exhibited superior targeting to the tMCAO brain compared with the spleen (Figure 1M).

Taken together, the anti-CAM-targeted delivery systems tested in this study demonstrate consistent uptake patterns in the main organs. (1) CAM targeting resulted in higher brain accumulation than control IgG, with superior VCAM targeting to the brain being due to evasion of uptake by the lungs. (2) PECAM targeting resulted in similar lungs accumulation in both healthy and tMCAO mice. (3) ICAM counterparts accumulated preferably in the injured brain hemisphere, as well as in the lungs. These studies showed that targeting to PECAM, ICAM, or VCAM can enhance tMCAO brain uptake of liposomes and LNPs. Specifically, VCAM targeting produced the best tMCAO brain delivery by nearly every metric, exceeding untargeted NCs by one to two orders of magnitude. Therefore, additional experiments in this study focused on VCAM targeting.

VCAM-targeted NCs deliver to the endothelial cells and leukocytes of the tMCAO brain

Having shown strong brain uptake of VCAM-targeted NCs, we next sought to determine which cell types in the brain were responsible for this delivery. We injected fluorophore-labeled, VCAM-targeted liposomes IV into tMCAO mice, then harvested and disaggregated the brain to create a single cell suspension, following the experimental timeline in Figure 1A. Cells were stained with CD31 and CD45 to identify target cell types: endothelial cells (CD31⁺/CD45⁻) and leukocytes (CD45⁺/CD31⁻). Double-negative cells were not further subtyped. Flow cytometry showed an increase in the total leukocyte population in the ipsilateral ischemic brain (Figure S4), consistent with published observations in the tMCAO mouse model illustrating inflammation in AIS.^{30,31} VCAM-targeted liposomes were preferentially taken up by endothelial cells (Figures 2A–2D) and leukocytes (Figures 2E–2H) in tMCAO brains. In the ipsilateral hemisphere, liposome uptake was enhanced in both endothelial cells and leukocytes, compared with the contralateral hemisphere. The number of recovered endothelial cells (Figure 2C) and leukocytes (Figure 2G) that were liposome positive trended toward higher values in the ipsilateral hemisphere. Liposome fluorescence intensity in both endothelial cells (Figure 2D) and leukocytes (Figure 2H) was significantly higher in the ipsilateral hemisphere, as compared with the contralateral.

Next, we characterized the distribution of the cargo after VCAM-targeted NCs delivery. Mass spectrometry imaging (MSI) is a powerful tool enabling investigations into the spatial distribution of molecular species, including small molecule drugs. Having shown VCAM-targeted NC delivery to brain endothelial cells and leukocytes, we reasoned that VCAM targeting would be well-suited to delivery of therapeutic cargoes for treatment of AIS, especially anti-inflammatory agents.³² For small molecule drug delivery by liposomes, we chose dexamethasone-21-phosphate (Dex), a glucocorticoid with anti-inflammatory effects on endothelial cells and leukocytes.^{33,34} We hypothesized that VCAM-targeted liposomes would deliver and concentrate Dex in the ipsilateral hemisphere. Dex was loaded into liposomes through passive loading method as previously described,²³ with an entrapment efficiency of $13.8 \pm 0.7\%$, and drug/lipid ratio of 0.26 g of Dex/g lipid (Table 1). We IV injected VCAM-targeted liposomes encapsulated with Dex into tMCAO mice 24 h after injury and allowed them to circulate for 30 min. Brain uptake of Dex-containing liposomes was not significantly different from empty liposomes (Figure S5). Consecutive brain sections were obtained for MSI or cresyl violet staining to visualize neurons (stained in purple). The top image in Figure 2I showed neuronal death in the infarct area (white, black dashed circles) in tMCAO-challenged mice, compared with naive animal. MSI demonstrated a higher concentration of Dex in the ipsilateral (injured) region of the ipsilateral brain more than in the contralateral (Figures 2I and S6).

For mRNA delivery by LNPs, we performed studies of gene editing by VCAM-targeted LNPs loaded with mRNA encoding for Cre-recombinase (Table 1) to alter tdTomato (fluorophore) expression in reporter mice.³⁵ These mice express robust tdTomato after Cre-mediated recombination. To visualize the spatial distribution of

transfected cells, we employed the CLARITY tissue imaging technique, which transforms the intact tissue into a hydrogel-tissue hybrid by removing of lipids while preserving the intact anatomical structure, proteins, and nucleic acids for imaging.³⁶ After three doses of anti-VCAM LNPs, we characterized distribution of transfected cells over the whole brain (Figure 2J) and Videos S1–S4). We observed, in Ai9 mice, tdTomato expression mainly in the brain vasculature in the whole brain. By immunohistology, we identified transfection of both infiltrated leukocytes and endothelial cells in mTmG mice, as shown in Figures 2K and S7. The arrow in the top row of Figure 2K captured the infarct core (sparse cell distribution and debris of CD31 signal for endothelium) and the penumbra area (more intact CD31 staining). The transfected endothelial cells were found in both areas. The bottom row of Figure 2K shows transfection co-localized with CD45 signal, indicating infiltrated leukocytes in the infarct core. To the best of our knowledge, this is the first report describing the delivery of mRNA-LNP in a stroke animal model showing effective delivery mRNA encoding gene editing proteins (Cre-recombinase).

VCAM-targeted immunoliposomes deliver small molecule drug to the ischemic brain and reduce infarct volume

Dex is well established as a treatment for decreasing inflammatory brain injury, but was not clinically effective in decreasing infarct volume in AIS patients,^{37,38} possibly due to the limited amount of drug delivered to the lesion.^{39,40} By loading Dex into anti-VCAM liposomes, we hypothesized that it would be concentrated in endothelial cells and leukocytes, ameliorating local inflammation and decreasing the infarct size in the tMCAO model.

In tMCAO mice, we IV injected anti-VCAM liposomes loaded with Dex, empty anti-VCAM liposomes, or free Dex at a drug dose of 0.5 mg/kg directly after reperfusion, and then two additional doses at 24-h intervals. Drug effects were determined at day 3 after reperfusion (Figure 3A). In mice that only received an IV injection of the vehicle control, we observed that the infarct volume increased by 61% between 24 h and 72 h (Figure S8), as assessed by tetrazolium chloride (TTC) staining showing metabolically active and inactive tissues and consistent with previous observations showing the penumbra around the ischemic core slowly dies. No significant effects on infarct size were detected for free Dex or for empty anti-VCAM liposomes, but anti-VCAM liposomes loaded with Dex reduced infarct volume by $35.0 \pm 4.8\%$ (Figure 3B). Mice receiving free Dex had 50% survival vs. 85% in anti-VCAM Dex-liposomes (Figure 3C). Infarct volume in mice that received anti-VCAM Dex-liposomes at 72 h was essentially identical to infarct volume at 24 h after injury in mice that received the vehicle control (79.8 mm^3 vs. 75.8 mm^3 ; $p = 0.9578$). These results suggest that the anti-VCAM Dex-liposomes fully arrest infarct volume expansion from 24 to 72 h.

VCAM-targeted LNPs deliver mRNA to the ischemic brain and ameliorate tMCAO-induced brain injury

LNPs have showed great potential in delivering RNA, but few studies have shown therapeutic efficacy of LNPs for ischemic stroke.

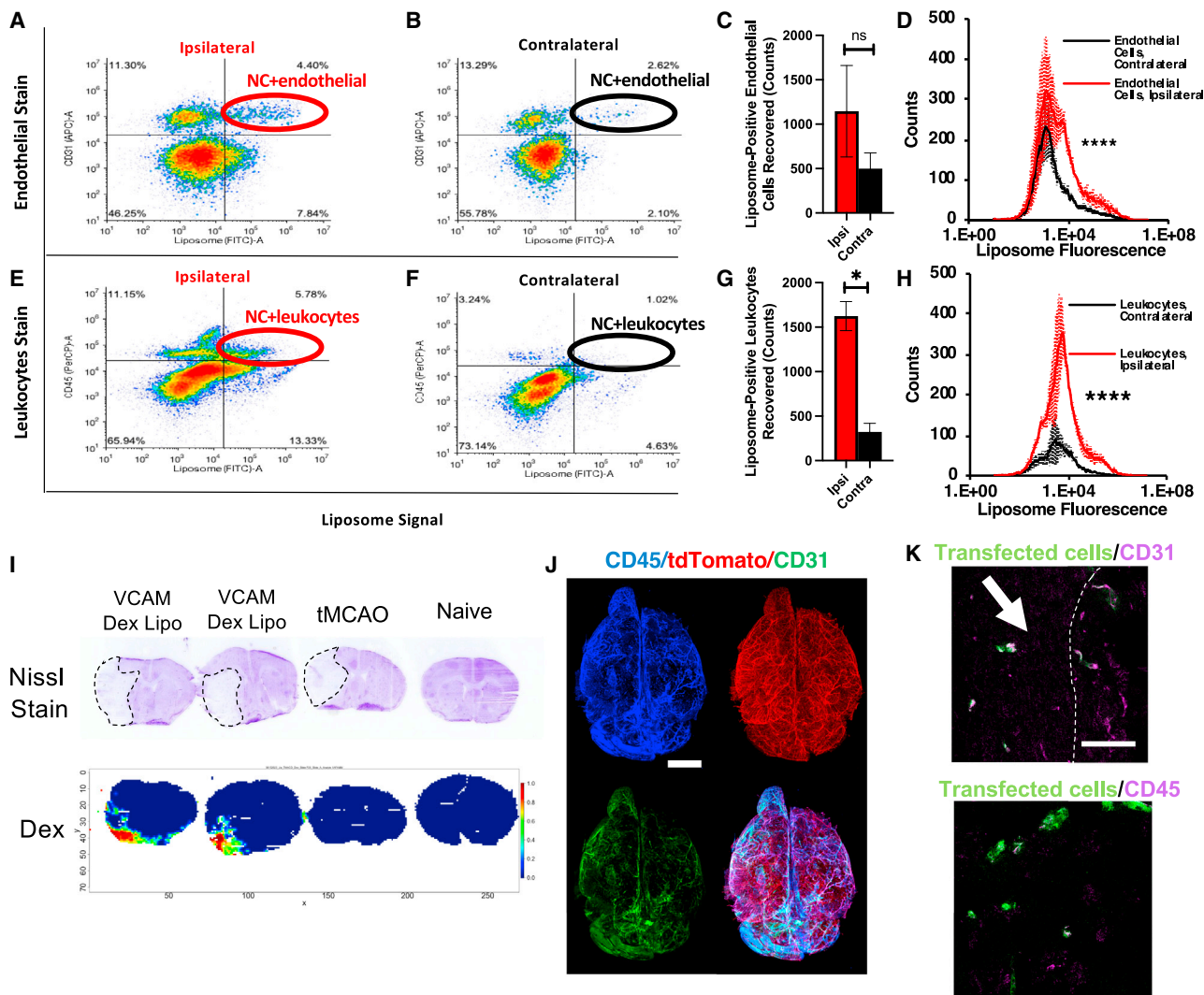


Figure 2. VCAM-targeted NCs localize to endothelial cells and leukocytes in tMCAO brains and concentrate cargos in ipsilateral hemisphere

(A–H) tMCAO mice were IV-injected with fluorophore-labeled VCAM-targeted liposomes, and single-cell suspensions were prepared from the brains 30 min later. Flow cytometry of the ipsilateral hemisphere shows higher VCAM-targeted liposome uptake in endothelial cells (CD31⁺/CD45⁺; [A] ipsilateral, [B] contralateral) and leukocytes (CD45⁺; [E] ipsilateral, [F] contralateral), compared with uptake in the contralateral hemisphere. The contralateral hemisphere had fewer total leukocytes infiltrate into the brain, compared with the ipsilateral hemisphere (E–F and H). Comparison of the contralateral (black) and ipsilateral (red) hemispheres in terms of the number of recovered endothelial cells (C) and leukocytes (G) that were liposome positive showed a trend toward more liposome-positive cells in the ipsilateral hemisphere, for both cell types, with *p < 0.05 using Student's t-test. Comparison of liposome fluorescence intensity in endothelial cells (D) and leukocytes (H) of the ipsilateral (red) vs. contralateral (black) brain showed higher liposome uptake in both cell types in the ipsilateral brain. ****p < 0.0001 using Kolmogorov-Smirnov test. n = 4. (I) Cresyl violet staining of brain slices from tMCAO mice treated with or without VCAM-targeted liposomes loaded with dexamethasone (dex), from untreated tMCAO mice, and from naive mice. MSI of dex in the consecutive slices. (J) Whole-brain CLARITY images in Ai9 mice show leukocytes (CD45, blue), cells transfected by VCAM-targeted LNP/Cre-recombinase mRNA treatment (tdTomato, red), and endothelial cells (CD31, green). Scale bar, 3,000 μ m. (K) Confocal image of brain from tMCAO mTmG mice injected with VCAM-targeted LNP-Cre-recombinase mRNA. Transfected cells switch from tdTomato to GFP (Figure S6A). Dashed line split the core/penumbra area and the arrow indicates the core of injury. Endothelial cells (CD31⁺) were transfected in both infarct core and penumbra (top), and infiltrated leukocytes (CD45⁺) in the infarct core were transfected (bottom). Scale bar, 100 μ m.

Different from the delivery of small molecule drugs, which allows potential drug diffusion to neighboring cells or surrounding tissue within minutes, the delivery of mRNA provides protection beginning hours after injection that may persist for up to 24 days.⁴¹ First, we tested functional activity of VCAM-targeted LNP in tMCAO mice af-

ter systemic delivery (IV). To assess reporter transgene expression, we IV injected anti-VCAM LNP and IgG control LNP containing luciferase mRNA (8 μ g RNA) (Table 1) into tMCAO mice 24 h after injury and into naive mice. Four hours after LNP injection, anti-VCAM LNP produced significantly higher levels of luciferase than untargeted

Table 1. Characterization of targeted NCs

	VCAM-dex-liposome	IgG-luciferase LNP	VCAM-luciferase LNP	VCAM-Cre recombinase LNP	Control IL-10 LNP	VCAM-IL-10 LNP
Size (nm)	161 ± 2	111 ± 0.1	115 ± 0.1	107 ± 3	78 ± 0.25	102.5 ± 0.9
PDI	0.15 ± 0.03	0.09 ± 0.01	0.10 ± 0.03	0.08 ± 0.01	0.04 ± 0.01	0.12 ± 0.01
Zeta potential (mV)	-4.5 ± 0.1	-5.3 ± 0.8	-5.8 ± 0.1	-5.5 ± 0.71	-6.1 ± 0.3	-6.0 ± 0.5
Drug loading, %	13.8 ± 0.7	95.8 ± 0.2	95.8 ± 0.2	94.2 ± 0.03	96.1 ± 1.2	96.1 ± 1.2%

n = 3. All values represented as mean ± SEM of three independent measurements.

IgG LNPs. VCAM targeting improved luciferase expression, especially in tMCAO brains (Figures 3D and S9).

Encouraged by the selective expression of luciferase using VCAM-targeted LNPs in tMCAO brain, we examined the therapeutic effect of these LNP loaded with mRNA encoding for IL-10 (Table 1). IL-10 is a potent anti-inflammatory cytokine and has been reported to down-regulate inflammatory signals and mediate neuroprotection.^{42,43} The expression and secretion kinetics of IL-10 into the cell culture media was first confirmed by treating RAW 264.7 macrophages with LNP/IL-10 (Figure S10). Continuous secretion was observed over 24 h. IV injection of three doses of IL-10 mRNA containing anti-VCAM LNP (anti-VCAM LNP/IL-10 mRNA, 8 µg mRNA per dose) after reperfusion (Figure 3A) decreased the infarct volume by 62.1 ± 13.4%, while the untargeted control (bare) counterpart did not show a significant therapeutic effect (Figure 3E). Immunostaining of LNP/IL-10 mRNA-treated brain sections showed that IL-10-expressing endothelial cells were found only in VCAM-LNP/IL-10 mRNA-treated animals, but not in the control LNP/IL-10 mRNA group (Figures 3F and S11). Mice receiving anti-VCAM LNPs/IL-10 mRNA had 100% survival (Figure 3G). VCAM targeting improved side effects associated with untargeted LNPs (Figure S15). IL-10 plasma concentrations were significantly elevated after treatment with VCAM-targeted/IL-10 mRNA containing LNPs, but higher IL-10 plasma levels were achieved with non-targeted control LNPs (Figures 3H and S12). We note that VCAM targeting shifts the LNP biodistribution, decreasing liver uptake and plasma retention (Figure S1C). This may account for the higher levels of IL-10 in the liver and plasma with non-targeted (Figure S9 for liver expression). Among other tested cytokines, only monocyte chemoattractant protein-1 (Figure S12) significantly differed among untreated, control LNP and targeted LNP groups. Additional studies were performed to elucidate the impact of anti-VCAM LNPs containing IL-10 mRNA on the leukocyte population in the brain. Flow cytometry of brain single cell suspensions revealed a decreased abundance of leukocytes (CD45⁺) and macrophages/microglia (CD45⁺/CD11b⁺/F4/80⁺) (Figure 3I). A detailed analysis of neutrophils (CD45⁺/Ly6G⁺) showed a decrease in neutrophil activation, quantified by the median fluorescent intensity of CD11b (Figure S13A).⁴⁴ However, anti-VCAM LNPs/IL-10 mRNA did not affect the relative abundance of pro-inflammatory M1-polarized macrophages (inducible nitric oxide synthase [iNOS]; iNOS⁺CD206⁻), and significantly decrease anti-inflammatory M2-polarized macrophages (iNOS⁻CD206⁺) (Figure S13B). Despite the unexpected decrease of M2 macrophage abun-

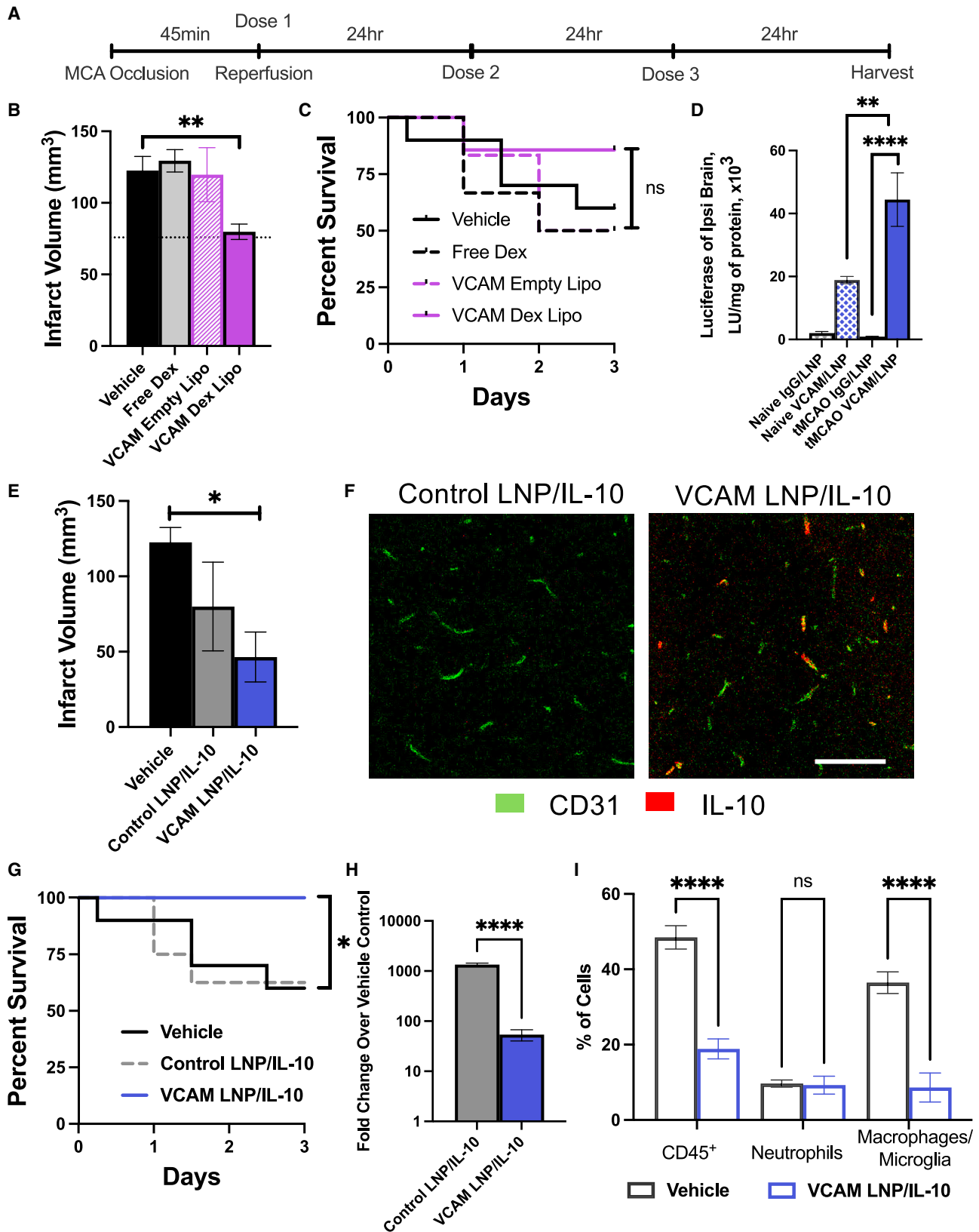
dance after the treatment, the decrease in the total macrophage/microglia population and of neutrophil activation suggests protection against inflammatory leukocyte infiltration when we target IL-10 mRNA delivery to the injured BBB.

DISCUSSION

More than 1,000 drugs have been tested in animal models of AIS and only one-third of them showed protective effects preclinically, resulting in more than 100 being tested in AIS patients. However, all clinical trials failed to improve outcomes.¹² The most frequently cited reason for failure was the inability to achieve efficacious concentrations of drugs in brain tissue without causing intolerable side effects. Only re-canalizing therapies (thrombolysis and thrombectomies) are efficacious for the treatment of AIS and tPA is the only drug approved by the U.S. Food and Drug Administration to restore blood flow in AIS.³⁻⁵ Accordingly, the death rate from stroke in the United States decreased by 77% between 1969 and 2013.⁴⁵ Despite this improvement, 50%–55% of stroke patients still become functionally dependent. This raises a central question: Why is it not enough to restore blood flow? Sustained inflammation for days to weeks after the initial ischemic event is likely at least part of the answer to this question.⁴⁶ A recent study has shown cerebral microvasculature inflammation upon AIS in both mice and humans.⁴⁷ We hypothesized that treating sustained inflammation after AIS may improve stroke outcomes, but to do so, the therapeutic must be efficiently concentrated in the brain.

We aimed to develop NCs with the ability to deliver various therapeutics to specific locations in the brain affected by ischemic stroke. Our focus was on utilizing CAMs for this purpose. Previous studies employing microscopy and omics techniques have identified three main types of CAM expression in the brain: (1) pan-endothelial PECAM is constitutively expressed; (2) ICAM is normally present but upregulated in areas of inflammation and other pathologies; and (3) VCAM is modestly expressed under normal conditions, but strongly induced in pathological conditions.²⁰⁻²² However, the previously reported detection methods did not provide detailed information about the accessibility and anchoring capabilities of CAMs for drug delivery systems. To address this, ligands labeled with fluorophores, magnetic resonance imaging, or isotope probes offered a real-time assessment of the extent, kinetics, and duration of targeting these molecules.^{17,24}

It is essential to note that previous studies have not thoroughly investigated the accessibility of CAMs for targeted NCs using the chosen



(legend on next page)

model therapeutics. Moreover, the increase in intracranial pressure caused by vasogenic edema can decrease blood flow to the injured brain region, potentially impacting the delivery and local action of the cargo.⁴⁸ Each form of pathological process may have unique effects on drug delivery, and the cargo itself can affect the stability and other features of the drug delivery system. Therefore, our study aimed to address these challenges and provide novel insights into drug delivery system design, considering the role of the pathology and other factors involved.

Here, we demonstrated delivery to the ischemic hemisphere of IV-injected mAbs and the two most clinically relevant targeted NCs (liposomes and LNPs) directed to different CAMs. Targeting to the BBB via endothelial surface marker CAMs allows us to develop intervention strategies that correct BBB deficits by restoring its barrier function and reducing leukocyte infiltration that perpetuate the inflammatory process, enhancing the further disruption of the BBB and the formation of vasogenic edema.⁴⁹ We tested targeting to PECAM, ICAM, and VCAM. Comparing targeted vs. non-targeted delivery to the AIS-injured region of the brain, CAM targeting yielded 37- to 120-fold increased uptake for mAbs, 11- to 50-fold increased uptake for liposomes, and 4- to 16-fold increased uptake for LNPs. In all cases, VCAM targeting yielded the highest uptake in the injured hemisphere of the brain. This positions VCAM as the most attractive target for drug delivery in AIS.

Agreeing with previous studies, flow cytometry analysis of brains from tMCAO mice showed a marked influx of leukocytes in the injured brains.⁵⁰ This elevated influx was reduced after our therapeutic approach (Figure 3I). VCAM-targeted liposomes bound to endothelial cells, in agreement with prior studies,¹⁷ and accumulated the drug in the injured region of the brain as shown by MSI (Figure 2I). Cre-recombinase demonstrates the vascular accumulation of the LNPs with a higher density of edited vessels in the penumbra area. Histological analysis further confirmed the gene editing capability on both endothelial cells and leukocytes using VCAM-targeted LNPs (Figure 2K). This delivery feature is advantageous, as overzealous leukocytes in the injured region of the brain after stroke are known to be associated with poor patient outcomes.^{51,52} By providing delivery to the two main cell types driving post-stroke inflamma-

tion—endothelial cells and leukocytes—VCAM-targeted NCs are likely able to address this underlying mechanism of secondary injury and protracted cell death that occurs in the penumbra around the ischemic core.⁵³ Knowledge of the cell types responsible for delivery to the brain in tMCAO mice was useful in making informed decisions for what drug to test as a therapeutic.

We demonstrated that VCAM-targeted NCs can be used to deliver pharmacologically-relevant concentrations of small molecule drugs (liposomes) and mRNA (LNPs) at the inflamed region of the brain (Figure 1 by radiotracing; Figure 2 by MSI and CLARITY), showing the versatility of this targeting strategy. Small molecule drugs can be delivered to specific cells within minutes, as well as diffuse to surrounding cell and tissue to provide protection. Thus, it is considered “early protection.” In contrast, transcription and protein synthesis after mRNA delivery takes hours, but the effect can last from 24 h to days,⁴¹ which is considered “delayed protection.” To attack post-stroke inflammatory injury, we selected anti-inflammatory drugs Dex and mRNA encoding for IL-10 as cargo drugs to be used with VCAM-targeted NCs.

Dex is a glucocorticoid with anti-inflammatory effects on both endothelial cells and leukocytes and is relatively easy to encapsulate into targeted NCs.²⁵ It has effects on both endothelial cells and leukocytes by downregulating inflammatory signals,⁵⁴ potentially transforming the pro-inflammatory environment of the ischemic penumbra into an anti-inflammatory one. Dex was previously tested as a free drug in clinical trials to treat AIS, but failed due to lack of clear therapeutic benefits; it also induced severe systemic side effects.^{55,56} For all these reasons, we loaded Dex into VCAM-targeted liposomes. We found that VCAM-targeted Dex liposomes reduced infarct volume by 35% vs. vehicle control and free drug ($p = 0.02$ and 0.049 , respectively). In contrast with the free drug, we observed no brain hemorrhagic transformation and no gastrointestinal bleeds (Figure S14).

IL-10 is a potent cytokine with multifaceted anti-inflammatory properties that play a crucial role in the resolution of inflammation after AIS. IL-10 has been investigated in clinical trials for its potential therapeutic use in chronic inflammatory diseases. In the context of AIS, IL-10 is essential for resolving the inflammatory phase and promoting

Figure 3. VCAM-targeted NCs improved stroke outcomes

(A) Mice were treated with VCAM-targeted NCs loaded with the anti-inflammatory drug dexamethasone (Dex) or IL-10 mRNA, or various controls. Each animal received three IV injections: one immediately after tMCAO reperfusion, then two doses every 24 h thereafter. Mice were euthanized at 72 h and the infarct volume was measured post-mortem by staining for dead brain tissue. (B) Among the survived animals, VCAM-targeted liposomes loaded with Dex reduced stroke volume at 72 h, relative to all controls. Neither free Dex (no NC) nor empty VCAM-targeted liposomes decreased stroke volume. Dashed line: infarct volume at 24 h after tMCAO. (C) Dex-loaded VCAM targeted liposomes showed a higher but non-significant survival rate. For (B) and (C), $n = 10$ for control and $n = 6$ for the treatment groups, due to additional control in each cohort. (D) Luciferase expression in the naive or ipsilateral tMCAO brain showed elevated luciferase level after IV injection of VCAM-targeted LNP, compared with untargeted IgG control, and was improved especially in tMCAO brains. $**p < 0.01$, $****p < 0.0001$ using one-way ANOVA followed by Tukey's *post hoc*. $n = 4$. (E) IL-10 mRNA-loaded VCAM targeted LNP reduced stroke volume by 62.1%, while untargeted control (bare) LNP had no significant treatment effect. $n = 10$ for untreated control, $n = 8$ for control LNP/IL-10 and VCAM-targeted LNP/IL-10. $*p < 0.05$ using one-way ANOVA followed by Dunnett's *post hoc*. (F) IL-10 expression was detected in endothelial cells in tMCAO brain ipsilateral hemisphere with VCAM LNP/IL-10 mRNA treatment, but not with control LNP/IL-10 mRNA. Full panel shown in Figure S14. Scale bar, 100 μm . (G) IL-10 mRNA-loaded VCAM targeted LNP significantly improved the survival rate. $*p < 0.05$ using a log rank test. (H) Elevation of plasma IL-10 concentration following treatment LNP loaded with IL-10 mRNA. $n = 4$. $****p < 0.0001$ using Student's *t*-test. (I) VCAM LNP/IL-10 treatment leads to significant reduction of CD45⁺ cells and macrophage/microglia. $n = 3$. $****p < 0.0001$ using two-way ANOVA followed by Sidak's test. Data are presented as mean \pm SEM.

neuronal and glial cell survival.^{42,57} Human studies have indicated that low plasma levels of IL-10 are associated with poorer prognoses and outcomes in patients with AIS.⁵⁸ In contrast to prior studies using adeno-associated virus injected prior to the injury, and in some cases by intraparenchymal injections,⁵⁹ we injected VCAM-targeted mRNA LNP after the reperfusion occurs, mimicking the thrombectomy scenario. We observed a 62% decrease in infarct volume and a 100% survival rate with no bleeding or lung damage in mice receiving this treatment. This was in part due to the 2.6-fold decrease in the total infiltrated leukocytes, 4.2-fold decrease in total macrophages/microglia, and reduced activation of the infiltrated neutrophils. Untargeted (control) LNPs containing IL-10 mRNA also resulted in a much higher rate of mortality (37.5 %) and a 25-fold higher plasma concentration of IL-10 vs. the VCAM targeted one, probably due to the mainly liver uptake that is 2-fold higher for the untargeted therapy vs. the targeted one (Figure S1C; Table S4). We also observed that 25% of mice treated with untargeted LNP/IL-10 experienced lung injury and aqueous intestines, in contrast with the targeted LNP group (Figure S15). These results suggest that, rather than achieving high concentrations of IL-10 in the systemic circulation, enhancing local concentrations of IL-10 is more likely to enhance outcomes in AIS.

Among drugs that made it to AIS clinical trials, the average improvement in infarct volume in rodents was 25%,¹² so our result with VCAM targeting is promising. In fact, VCAM-targeted Dex-liposomes brought the infarct volume at 72 h down to the same level observed at 24 h in mice that received vehicle only. This suggests that VCAM-targeted Dex-liposomes accumulate in the injury site and can abrogate neuronal death in the inflammatory penumbra. In addition, we observed that we can target LNP to the ischemic brain for RNA delivery, which opens a new, nearly endless set of opportunities for delivery of mRNA encoding for therapeutic proteins without the need to significantly optimize LNP formulations.

In summary, this study uses the tMCAO model of AIS to show that targeting CAMs, especially VCAM, with mAbs and NCs is a promising direction for improvement of AIS therapies. VCAM-targeted NCs and mAbs accumulate in the AIS brain at levels one to two orders of magnitude higher than untargeted controls, concentrating the drug in the ischemic brain. VCAM targeting delivers NCs to key cell types involved in post-stroke inflammation, namely, endothelial cells and leukocytes. VCAM-targeted LNP are able to transfect and express mRNA in the ischemic brain. VCAM-targeted Dex-loaded liposomes reduced stroke size to a greater extent than most drugs that have moved from rodent to human studies. Thus, VCAM-targeted therapeutics represent an attractive platform for treating AIS.

MATERIALS AND METHODS

Reagents

All lipids for liposome preparation were purchased from Avanti Polar Lipids (Alabaster, AL). LNPs were provided by Acuitas Therapeutics (Vancouver, Canada). Dibenzocyclooctyne (DBCO)-PEG4-NHS ester was purchased from Click Chemistry Tools (Scottsdale, AZ).

Na¹²⁵I was purchased from PerkinElmer (Waltham, MA). Rat IgG and antibodies for flow cytometry were purchased from Invitrogen (Carlsbad, CA). Anti-mouse-PECAM-1 (clone MEC13.3) was purchased from BioLegend (San Diego, CA). All other chemicals and reagents were purchased from SigmaAldrich (St. Louis, MO), unless otherwise noted.

Animals

All animal studies were carried out in accordance with the *Guide for Care and Use of Laboratory Animals* under the protocol approved by the University of Pennsylvania Institutional Animal Care and Use Committee, and conformed to all relevant regulatory standards. All animal experiments were carried out using male, 6- to 8-week-old C57BL/6 mice (20-25 g) from Jackson Laboratories (Bar Harbor, ME), unless otherwise noted. Ischemic stroke was induced using the tMCAO model.⁶⁰ Mice were randomly assigned to groups and anesthetized with isoflurane. After proper anesthetic depth was verified, the mouse was placed on a heating pad with rectal temperature maintained at 37°C. The carotid artery was exposed under a dissecting microscope. A small arteriotomy was made and a filament was threaded into the MCA. A Doppler probe was put over the MCA. A more than 70% reduction of MCA blood flow was confirmed by Doppler ultrasound examination as the criteria for successful MCAO. Forty-five minutes later, the filament was removed, MCA blow flow return was confirmed by Doppler ultrasound examination, and hemostasis was achieved. More than 80% of blood flow restoration within 10 min after filament removal was required for animal inclusion in the study. The mouse was returned to its cage, and given 1 mL of normal saline subcutaneously to maintain hydration daily. Subsequently, food and water were provided on the floor of cage in a Petri dish.

Protein production and purification

Anti-mouse-VCAM-1 mAb (clone M/K2.7) and anti-mouse-ICAM-1 mAb (clone YN1/1.7.4) were produced by culturing hybridoma cells and purified using protein G sepharose chromatography (GE Healthcare Life Sciences, Pittsburgh, PA).

Antibody radiolabeling

Antibodies were radiolabeled with Na¹²⁵I using Pierce (Rockford, IL) Iodogen radiolabeling method. Briefly, tubes were coated with 100 µg Iodogen reagent. Antibody (1–2 mg/mL) and Na¹²⁵I (0.25 µCi/µg protein) were incubated for 5 min on ice. Unreacted materials were purified using Zeba 7 kDa desalting spin columns (Thermo Fisher Scientific, Waltham, MA). Thin-layer chromatography was used to confirm radiolabeling efficiency. All proteins were confirmed to have >90% radiochemical purity prior to use.

Antibody modification

Antibodies were functionalized with DBCO or N-succinimidyl S-acylthioacetate (SATA) for conjugation to liposomes or LNP, respectively, by reacting with a 5-fold molar excess of DBCO-PEG4-NHS ester or SATA for 30 min at room temperature. SATA deprotection was carried out with 0.5 M hydroxylamine. The unreacted compound

was removed via centrifugation using a molecular weight cutoff filter or G-25 Sephadex Quick Spin Protein columns (Roche Applied Science, Indianapolis, IN).

Liposome preparation

Azide functionalized liposomes were prepared by thin film hydration techniques, as previously described.⁶¹ Briefly, 1,2-dipalmitoyl-sn-glycero-3-phosphocholine (DPPC), cholesterol, and 1,2-distearoyl-sn-glycero-3-phosphoethanolamine-N-[azido(polyethyleneglycol)-2000 (DSPE-PEG2000-azide) were mixed in a molar ratio of 54:40:6. For flow cytometry studies, fluorescent liposomes were prepared by doping in a 0.1% molar ratio of TopFluor PC into the lipid film. The lipid film was rehydrated in phosphate-buffered saline (PBS), pH 7.4. To form drug-loaded liposomes, the lipid film was hydrated in a solution containing 40 mg/mL of Dex in PBS, pH 7.4. The resulting vesicles were extruded through 200 nm polycarbonate membranes. The drug entrapment efficiency was assessed using reversed phase high-performance liquid chromatography (HPLC), using a mobile phase containing 30% v/v acetonitrile, 70% v/v water, and 0.1% v/v trifluoroacetic acid and running through a C8 column (Eclipse XDB-C8, 3 μ m, 3.0 \times 100 mm, Phenomenex) at a flow rate of 0.6 mL/min. Dex was detected using UV absorbance at 240 nm.

Preparation of mRNA-LNP

mRNAs were produced as described previously⁶² using T7 RNA polymerase (Megascript, Ambion) on linearized plasmids encoding codon-optimized NanoLuc Luciferase (Promega), Cre recombinase, or murine IL-10 (NCBI Reference Sequence: NP_034678.1). To make modified nucleoside-containing mRNA, m¹ Ψ -5'-triphosphate (TriLink) was incorporated instead of UTP. mRNAs were transcribed to contain 101 nucleotide-long poly(A) tails. They were capped using the m7G capping kit with 2'-O-methyltransferase (ScriptCap, CellScript) to obtain cap1. mRNA was purified by Fast Protein Liquid Chromatography (FPLC) (Akta Purifier, GE Healthcare).⁶³ All prepared RNAs were analyzed by electrophoresis using denaturing or native agarose gels and stored at -20°C . FPLC-purified m¹ Ψ -containing NanoLuc luciferase and Cre-encoding mRNAs were encapsulated in LNP using a self-assembly process as previously described in which an aqueous solution of mRNA at acidic pH is rapidly mixed with a solution of lipids dissolved in ethanol.⁶⁴

The lipids and LNP composition are described in US patent US10,221,127, and mRNA-LNPs were prepared as previously described,^{26,65} and stored at -80°C at a concentration of mRNA of approximately 1 mg/mL. Before use, LNP were modified with DSPE-PEG(2000)-maleimide via a post-insertion technique.⁶⁶ Briefly, maleimide-functionalized micelles were prepared by mixing DSPE-PEG(2000) and DSPE-PEG(2000)-maleimide at a molar ratio of 4:1. Solvent was evaporated and the lipids were rehydrated in PBS at 65°C with vortex. Size of the micelles was 14–20 nm measured by dynamic light scattering. The desired amount of micelles were then mixed with 1 mg/mL of LNP and incubated for 3 h at 37°C to obtain maleimide-functionalized LNP for antibody conjugation.

Antibody conjugation

To conjugate targeting ligands, azide-functionalized liposomes were incubated with DBCO-modified antibodies at 4°C overnight with rotation. For targeted LNP, SATA-antibodies were conjugated to LNP particles via SATA-maleimide conjugation chemistry for 30 min at room temperature. Cystine was added to stop the SATA-maleimide reaction. For experiments involving radiotracing, ¹²⁵I-labeled untargeted rat IgG was spiked in at 10% of the total antibody mass added. Immunoliposomes and immunoLNP were purified using gel filtration chromatography to remove unbound antibodies. The size, distribution, and concentration of the NCs were determined using dynamic light scattering using Zetasizer Nano ZS (Malvern Instruments Ltd, Malvern, UK) and nanoparticle tracking analysis using a Nanosight NS300 (Malvern Panalytical, Westborough, MA). Antibody conjugation was measured using fluorescently labeled antibodies and purified using a size exclusion column (Sephadex). Efficiency of conjugation reaction is quantitatively defined as the ratio of the area under the curve of the ligand signal in the liposomal peak (5–7 mL) over the integration of the entire 25 mL elution. The conjugation efficiency for targeted liposomes is approximately 85%, and for targeted LNP approximately 95%, resulting in approximately 50 mAb/NC.

Biodistribution

For radiotracing experiments, mice were injected IV with radiolabeled antibody (5 μ g, approximately 0.2 mg/kg), immunoliposomes (10 mg/kg lipid, approximately 6E11 liposomes/animal), or LNPs (8 μ g of mRNA, approximately 0.32 mg/kg) 24 h post-tMCAO reperfusion. Thirty minutes after injection, animals were sacrificed and perfused with 20 mL of ice-cold PBS. Blood was collected in EDTA-coated tubes. Tissue distribution of injected materials was determined by measuring the radioactivity in the blood and other organs using a Wizard 2470 gamma counter (PerkinElmer, Waltham, MA). Tissue uptake was presented as percent injected dose normalized to the mass of tissue (%ID/g tissue).

Luciferase transfection

Transgene expression was assessed in mice following injection of LNP-NanoLuc mRNA and tissues were harvested 5 h post-injection and frozen at -80°C . Tissues were homogenized with 1 mL of Luciferase Cell Culture Lysis (Promega) containing protease inhibitor cocktail using PowerLyser 24 (Qiagen) and mixed gently at 4°C for 1 h. The homogenates were then subjected to cycles of freeze/thaw in dry ice/ 37°C . The resulting cell lysate was centrifuged for 10 min at 16,000 g at 4°C and supernatants were separated. Protein concentration was measured by Lowry assay. Luciferase activity was measured in supernatant using Nano-Glo Dual-Luciferase Reporter Assay System (Promega). Luminescence was assayed using a Victor³ 1420 Multilabel Plate Counter (PerkinElmer, Wellesley, MA). The data were presented as luminescence units normalized by mg of protein.

IL-10 expression assay

The expression of IL-10 was confirmed *in vitro* and *in vivo*. For *in vitro* expression, IL-10 mRNA or luciferase mRNA containing LNP was added to RAW 264.7 macrophages at the concentration of

400 ng/mL. At 6 h and 24 h, cell culture media was collected for IL-10 measurement. For *in vivo* expression, 3 doses of VCAM-LNP/IL-10 mRNA or control LNP/IL-10 mRNA was injected into tMCAO mice at 8 µg/dose. Before sacrificing, animals were injected with 5 µg of Alexa Fluor 647-labeled CD31 (Biolegend). Brain was then harvested and sectioned for immunostaining. The sections were fixed, permeabilized in 0.1% Triton X-100, and incubated with IL-10 primary antibody (1:200, Invitrogen) at 4°C overnight. After washing, the sections incubated with secondary antibody conjugated to Alexa fluorophores (1:500, Invitrogen) at room temperature for 2 h, then counterstained with nuclear dye 4'-6-Diamidino-2-phenylindole (DAPI, Southern Biotech, Birmingham, AL), imaged with Leica Stellaris 5 confocal microscopy.

Flow cytometry

To obtain single cell suspensions, brains were disaggregated as previously described.⁵⁰ Briefly, tissue was enzymatically digested with dispase at 37°C for 1 h, followed by addition of 600 U/mL DNase Grade II. Tissue digests were demyelinated using a Percoll gradient. Residual red blood cells were lysed by ACK buffer (Quality Biological, Gaithersburg, MD).

For liposome uptake analysis, cells were stained to determine the cellular distribution of VCAM-targeted liposomes in leukocytes (CD31⁺/CD45⁺) vs. endothelial cells (CD31⁺/CD45⁻) (Table S5). Flow cytometry was performed using an Accuri C6plus (Benton Dickinson, San Jose, CA).

To evaluate the therapeutic effect, leukocyte infiltration and inflammation/polarization state after VCAM LNP/IL-10 treatment was evaluated by flow cytometry using a CytoFLEX LX (Beckman Coulter, IN) (Table S6).

Histology

B6.129(Cg)-Gt(ROSA)26Sor^{tm4(ACTB-tdTomato,-EGFP)Luo/J} mice with two-color fluorescent Cre-reporter allele (mTmG mice), or B6.Cg-Gt(ROSA)26Sor^{tm9(CAG-tdTomato)Hze/J} with tdTomato Cre-reporter allele (Ai9 mice) (Jackson Laboratory, Farmington, CT) were used to determine the functional activity of mRNA/LNP. tMCAO animals were IV injected daily with VCAM targeted Cre-recombinase encoding mRNA-loaded LNP for 3 days starting just after reperfusion. At the end of the study, the brain was harvested.

For immunohistology, frozen tissue was cryosectioned using cryostat Leica CM 1950 (Leica Biosystems, Nussloch, Germany). Tissue specimen was then fixed with paraformaldehyde, counterstained with DAPI (Molecular Probes, Thermo Fisher Scientific), and imaged with Leica DM6000 Widefield microscope.

For the CLARITY tissue imaging technique, the brain was fixed with paraformaldehyde, and sent to LifeCanvas Technologies (Cambridge, MA) for tissue processing, staining (CD31 and CD45), imaging, and analysis.

Nissl staining

Brain sections were fixed by 4% paraformaldehyde. 0.1% cresyl violet acetate was dissolve in deionized water and filtered before use. Sections were hydrated in water for 20 min, then stained in cresyl violet for 5 min. After brief rinse of water, sections were dehydrated in 100% Ethanol for 1 min, Xylene for 1 min, then mounted in Fluoromount-G (Southern Biotech).

MSI

tMCAO challenged mice were injected with VCAM-liposomes loaded with Dex (0.5 mg/kg) 24 h post injury. Thirty minutes later, animals were perfused with PBS, and the brains were freshly frozen for cryo-section. Sections from the four groups were mounted on glass slides, and analyzed by desorption electrospray ionization mass spectrometry at 100 µM spatial resolution with detection on a Waters Xevo G2-XS qToF instrument in positive detection mode. Ions for dexamethasone [M + H]⁺ (m/z 393.207728) and [M-HF + H]⁺ (m/z 373.2015) were detected in addition to a range of typically observed brain lipid peaks. The dexamethasone ion peaks were normalized to the molecular ion for PC 34:1 [M + K]⁺, the most abundant phosphatidylcholine species in brain tissue.

Therapeutic studies

To study the therapeutic effects, VCAM-targeted Dex-loaded liposomes or IL-10 mRNA loaded LNP were dosed IV every 24 h starting just after removal of the filament for a total of three doses prior to sacrifice and compared with their controls. Animals were perfused with ice-cold PBS and the brains were removed and sectioned into 1 mm thickness using a rotary hand microtome. The ischemic infarct was evaluated by immunohistochemical analysis using 1% TTC staining. The area of non-stained infarct in each slice was measured using ImageJ in a blinded manner. The ischemic infarct volume area was calculated and multiplied by slice thickness and summed.

Cytokine measurement

Plasma and cell culture media were collected after IL-10 mRNA containing LNP treatment. The LEGENDplex Mouse Inflammation Panel 13-plex (Biolegend) was used for cytokine quantification. Measurement was performed on an LSR Fortessa B flow cytometer (Becton Dickinson, Franklin Lakes, NJ) using LEGENDplex software for data analysis.

Statistics

All results are expressed as mean ± SEM. Statistical analyses were performed using GraphPad Prism 8 (GraphPad Software, San Diego, CA), where *p < 0.05, **p < 0.01, ***p < 0.001, and ****p < 0.0001.

DATA AND CODE AVAILABILITY

All data and materials supporting the findings of this manuscript are presented in the paper and/or the Supplemental information. Additional data are available from the corresponding authors upon reasonable request.

SUPPLEMENTAL INFORMATION

Supplemental information can be found online at <https://doi.org/10.1016/j.ymthe.2024.03.004>.

ACKNOWLEDGMENTS

J.N. received funding from the American Heart Association (Grant 916172). O.A.M.-C and P.M.G received funding from CT³N Pilot Grants from the Institute for Translational Medicine and Therapeutics of the University of Pennsylvania. O.A.M.-C. received funding from the American Heart Association (Grant 19CDA34590001). P.M.G. received funding from the National Institutes of Health K99 (K99HL153696). M.E.Z. received funding from the National Institutes of Health F31 (F31 HL154662-01). S.O. received funding from the American Heart Association (Grant 23PRE1014444). V.R.M and J.S.B. received support from the Cardiovascular Institute of the University of Pennsylvania. J.S.B. received funding from K08-HL-138269, R01-HL-153510, R01-HL-160694, R01-HL-157189, and R21-AI-166778-01. V.R.M received funding from the National Institutes of Health (NIH) (R01 HL155106, R01 HL128398, and R01 HL143806).

AUTHOR CONTRIBUTIONS

Study design: J.N., P.M.G., and O.A.M.C.; LNP preparation: V.V.S., M.A., Y.K.T., and B.L.M.; mRNA preparation: T.E.P. and H.P.; experiments and data acquisition: J.N., P.M.G., O.A.M.C., S.R., H.C.D., R.Y.K., S.O., M.E.Z., T.S., E.A., X.G., T.V.B., A.W.T., and A.G.W.; manuscript preparation: J.N., P.M.G., and O.A.M.C.; manuscript review and editing: J.N., P.M.G., O.A.M.C., H.C.D., J.W.M., S.E.K., C.A.T., T.E.P., A.W., H.P., V.R.M., and J.S.B.; funding acquisition: P.M.G., O.A.M., V.R.M., and J.S.B.

DECLARATION OF INTERESTS

J.N., P.M.G., V.V.S., H.P., D.W., J.S.B., V.R.M., and O.A.M.-C. have pending patent applications fully disclosed by the University of Pennsylvania.

REFERENCES

1. Donkor, E.S. (2018). Stroke in the 21(st) Century: A Snapshot of the Burden, Epidemiology, and Quality of Life. *Stroke Res. Treat*, 3238165. <https://doi.org/10.1155/2018/3238165>.
2. Tsao, C.W., Aday, A.W., Almarazooq, Z.I., Alonso, A., Beaton, A.Z., Bittencourt, M.S., Boehme, A.K., Buxton, A.E., Carson, A.P., Commodore-Mensah, Y., et al. (2022). Heart Disease and Stroke Statistics-2022 Update: A Report From the American Heart Association. *Circulation* 145, e153–e639. <https://doi.org/10.1161/CIR.0000000000001052>.
3. Albers, G.W., Marks, M.P., Kemp, S., Christensen, S., Tsai, J.P., Ortega-Gutierrez, S., McTaggart, R.A., Torbey, M.T., Kim-Tenser, M., Leslie-Mazwi, T., et al. (2018). Thrombectomy for Stroke at 6 to 16 Hours with Selection by Perfusion Imaging. *N. Engl. J. Med.* 378, 708–718. <https://doi.org/10.1056/NEJMoa1713973>.
4. Berkhemer, O.A., Fransen, P.S., Beumer, D., van den Berg, L.A., Lingsma, H.F., Yoo, A.J., Schonewille, W.J., Vos, J.A., Nederkoorn, P.J., Wermer, M.J., et al. (2015). A randomized trial of intraarterial treatment for acute ischemic stroke. *N. Engl. J. Med.* 372, 11–20. <https://doi.org/10.1056/NEJMoa1411587>.
5. National Institute of Neurological Disorders and Stroke rt-PA Stroke Study Group (1995). Tissue plasminogen activator for acute ischemic stroke. *N. Engl. J. Med.* 333, 1581–1587. <https://doi.org/10.1056/NEJM199512143332401>.

6. Nogueira, R.G., Jadhav, A.P., Haussen, D.C., Bonafe, A., Budzik, R.F., Bhuva, P., Yavagal, D.R., Ribo, M., Cognard, C., Hanel, R.A., et al. (2018). Thrombectomy 6 to 24 Hours after Stroke with a Mismatch between Deficit and Infarct. *N. Engl. J. Med.* 378, 11–21. <https://doi.org/10.1056/NEJMoa1706442>.
7. Rossi, B., Angiari, S., Zenaro, E., Budui, S.L., and Constantin, G. (2011). Vascular inflammation in central nervous system diseases: adhesion receptors controlling leukocyte-endothelial interactions. *J. Leukoc. Biol.* 89, 539–556. <https://doi.org/10.1189/jlb.0710432>.
8. Frijns, C.J., and Kappelle, L.J. (2002). Inflammatory cell adhesion molecules in ischemic cerebrovascular disease. *Stroke* 33, 2115–2122. <https://doi.org/10.1161/01.str.0000021902.33129.69>.
9. Okada, Y., Copeland, B.R., Mori, E., Tung, M.M., Thomas, W.S., and del Zoppo, G.J. (1994). P-selectin and intercellular adhesion molecule-1 expression after focal brain ischemia and reperfusion. *Stroke* 25, 202–211. <https://doi.org/10.1161/01.str.25.1.202>.
10. Yilmaz, G., and Granger, D.N. (2008). Cell adhesion molecules and ischemic stroke. *Neurol. Res.* 30, 783–793. <https://doi.org/10.1179/174313208X341085>.
11. Zhang, R., Chopp, M., Zhang, Z., Jiang, N., and Powers, C. (1998). The expression of P- and E-selectins in three models of middle cerebral artery occlusion. *Brain Res.* 785, 207–214. [https://doi.org/10.1016/s0006-8993\(97\)01343-7](https://doi.org/10.1016/s0006-8993(97)01343-7).
12. O'Collins, V.E., Macleod, M.R., Donnan, G.A., Horky, L.L., van der Worp, B.H., and Howells, D.W. (2006). 1,026 experimental treatments in acute stroke. *Ann. Neurol.* 59, 467–477. <https://doi.org/10.1002/ana.20741>.
13. Hou, X., Zaks, T., Langer, R., and Dong, Y. (2021). Lipid nanoparticles for mRNA delivery. *Nat. Rev. Mater.* 6, 1078–1094. <https://doi.org/10.1038/s41578-021-00358-0>.
14. Yu, B., Tai, H.C., Xue, W., Lee, L.J., and Lee, R.J. (2010). Receptor-targeted nanocarriers for therapeutic delivery to cancer. *Mol. Membr. Biol.* 27, 286–298. <https://doi.org/10.3109/09687688.2010.521200>.
15. Deddens, L.H., van Tilborg, G.A.F., van der Marel, K., Hunt, H., van der Toorn, A., Viergever, M.A., de Vries, H.E., and Dijkhuizen, R.M. (2017). In Vivo Molecular MRI of ICAM-1 Expression on Endothelium and Leukocytes from Subacute to Chronic Stages After Experimental Stroke. *Transl Stroke Res.* 8, 440–448. <https://doi.org/10.1007/s12975-017-0536-4>.
16. Licata, G., Tuttolomondo, A., Corrao, S., Di Raimondo, D., Fernandez, P., Caruso, C., Avellone, G., and Pinto, A. (2006). Immunoinflammatory activation during the acute phase of lacunar and non-lacunar ischemic stroke: association with time of onset and diabetic state. *Int. J. Immunopathol Pharmacol.* 19, 639–646. <https://doi.org/10.1177/039463200601900320>.
17. Gauberti, M., Montagne, A., Marcos-Contreras, O.A., Le Behot, A., Maubert, E., and Vivien, D. (2013). Ultra-sensitive molecular MRI of vascular cell adhesion molecule-1 reveals a dynamic inflammatory penumbra after strokes. *Stroke* 44, 1988–1996. <https://doi.org/10.1161/STROKEAHA.111.000544>.
18. Wang, Z., Zhou, W., Dong, H., Ma, X., and He, Z. (2018). Dexmedetomidine pretreatment inhibits cerebral ischemia/reperfusion-induced neuroinflammation via activation of AMPK. *Mol. Med. Rep.* 18, 3957–3964. <https://doi.org/10.3892/mmr.2018.9349>.
19. Krupinski, J., Kaluza, J., Kumar, P., Kumar, S., and Wang, J.M. (1994). Role of angiogenesis in patients with cerebral ischemic stroke. *Stroke* 25, 1794–1798. <https://doi.org/10.1161/01.str.25.9.1794>.
20. Vemuganti, R., Dempsey, R.J., and Bowen, K.K. (2004). Inhibition of intercellular adhesion molecule-1 protein expression by antisense oligonucleotides is neuroprotective after transient middle cerebral artery occlusion in rat. *Stroke* 35, 179–184. <https://doi.org/10.1161/01.STR.0000106479.53235.3E>.
21. Berti, R., Williams, A.J., Moffett, J.R., Hale, S.L., Velarde, L.C., Elliott, P.J., Yao, C., Dave, J.R., and Tortella, F.C. (2002). Quantitative real-time RT-PCR analysis of inflammatory gene expression associated with ischemia-reperfusion brain injury. *J. Cereb. Blood Flow Metab.* 22, 1068–1079. <https://doi.org/10.1097/00004647-200209000-00004>.
22. Lee, N.T., Selan, C., Chia, J.S.J., Sturgeon, S.A., Wright, D.K., Zamani, A., Pereira, M., Nandurkar, H.H., and Sashindranath, M. (2020). Characterization of a novel model of global forebrain ischaemia-reperfusion injury in mice and comparison with focal ischaemic and haemorrhagic stroke. *Sci. Rep.* 10, 18170. <https://doi.org/10.1038/s41598-020-75034-4>.

23. Nong, J., Glassman, P.M., and Muzykantov, V.R. (2022). Targeting vascular inflammation through emerging methods and drug carriers. *Adv. Drug Deliv. Rev.* *184*, 114180. <https://doi.org/10.1016/j.addr.2022.114180>.
24. Marcos-Contreras, O.A., Greineder, C.F., Kiseleva, R.Y., Parhiz, H., Walsh, L.R., Zuluaga-Ramirez, V., Myerson, J.W., Hood, E.D., Villa, C.H., Tombacz, I., et al. (2020). Selective targeting of nanomedicine to inflamed cerebral vasculature to enhance the blood-brain barrier. *Proc. Natl. Acad. Sci. USA* *117*, 3405–3414. <https://doi.org/10.1073/pnas.1912012117>.
25. Anderson, R., Franch, A., Castell, M., Perez-Cano, F.J., Brauer, R., Pohlers, D., Gajda, M., Siskos, A.P., Katsila, T., Tamvakopoulos, C., et al. (2010). Liposomal encapsulation enhances and prolongs the anti-inflammatory effects of water-soluble dexamethasone phosphate in experimental adjuvant arthritis. *Arthritis Res. Ther.* *12*, R147. <https://doi.org/10.1186/ar3089>.
26. Parhiz, H., Shuvaev, V.V., Pardi, N., Khoshnejad, M., Kiseleva, R.Y., Brenner, J.S., Uhler, T., Tuyishime, S., Mui, B.L., Tam, Y.K., et al. (2018). PECAM-1 directed re-targeting of exogenous mRNA providing two orders of magnitude enhancement of vascular delivery and expression in lungs independent of apolipoprotein E-mediated uptake. *J. Control Release* *291*, 106–115. <https://doi.org/10.1016/j.jconrel.2018.10.015>.
27. Nong, J., Glassman, P.M., Myerson, J.W., Zuluaga-Ramirez, V., Rodriguez-Garcia, A., Mukalel, A., Omo-Lamai, S., Walsh, L.R., Zamora, M.E., Gong, X., et al. (2023). Targeted Nanocarriers Co-Opting Pulmonary Intravascular Leukocytes for Drug Delivery to the Injured Brain. *ACS Nano* *17*, 13121–13136. <https://doi.org/10.1021/acsnano.2c08275>.
28. Ferguson, L.T., Ma, X., Myerson, J.W., Wu, J., Glassman, P.M., Zamora, M.E., Hood, E.D., Zaleski, M., Shen, M., Essien, E.O., et al. (2023). Mechanisms by Which Liposomes Improve Inhaled Drug Delivery for Alveolar Diseases. *Adv. Nanobiomed Res.* *3*, 2200106. <https://doi.org/10.1002/anbr.202200106>.
29. Wang, Z., and Brenner, J.S. (2021). The Nano-War Against Complement Proteins. *AAPS J.* *23*, 105. <https://doi.org/10.1208/s12248-021-00630-9>.
30. Zhou, W., Liesz, A., Bauer, H., Sommer, C., Lahrmann, B., Valous, N., Grabe, N., and Veltkamp, R. (2013). Postischemic brain infiltration of leukocyte subpopulations differs among murine permanent and transient focal cerebral ischemia models. *Brain Pathol.* *23*, 34–44. <https://doi.org/10.1111/j.1750-3639.2012.00614.x>.
31. Kim, H.A., Whittle, S.C., Lee, S., Chu, H.X., Zhang, S.R., Wei, Z., Arumugam, T.V., Vinh, A., Drummond, G.R., and Sobey, C.G. (2014). Brain immune cell composition and functional outcome after cerebral ischemia: comparison of two mouse strains. *Front Cell Neurosci* *8*, 365. <https://doi.org/10.3389/fncel.2014.00365>.
32. Lakhan, S.E., Kirchgessner, A., and Hofer, M. (2009). Inflammatory mechanisms in ischemic stroke: therapeutic approaches. *J. Transl Med.* *7*, 97. <https://doi.org/10.1186/1479-5876-7-97>.
33. Salvador, E., Shityakov, S., and Forster, C. (2014). Glucocorticoids and endothelial cell barrier function. *Cell Tissue Res* *355*, 597–605. <https://doi.org/10.1007/s00441-013-1762-z>.
34. Tsurufuji, S., Kurihara, A., and Ojima, F. (1984). Mechanisms of anti-inflammatory action of dexamethasone: blockade by hydrocortisone mesylate and actinomycin D of the inhibitory effect of dexamethasone on leukocyte infiltration in inflammatory sites. *J. Pharmacol. Exp. Ther.* *229*, 237–243.
35. Lee, L.R., Peacock, L., Lisowski, L., Little, D.G., Munns, C.F., and Schindeler, A. (2019). Targeting Adeno-Associated Virus Vectors for Local Delivery to Fractures and Systemic Delivery to the Skeleton. *Mol. Ther. Methods Clin. Dev.* *15*, 101–111. <https://doi.org/10.1016/j.omtm.2019.08.010>.
36. Du, H., Hou, P., Zhang, W., and Li, Q. (2018). Advances in CLARITY-based tissue clearing and imaging. *Exp. Ther. Med.* *16*, 1567–1576. <https://doi.org/10.3892/etm.2018.6374>.
37. Shaikh, A.K., Mohammad, Q.D., Ullah, M.A., Ahsan, M.M., Rahman, A., and Shakoor, M.A. (2011). Effect of dexamethasone on brain oedema following acute ischemic stroke. *Mymensingh Med. J.* *20*, 450–458.
38. Anderson, D.C., and Cranford, R.E. (1979). Corticosteroids in ischemic stroke. *Stroke* *10*, 68–71. <https://doi.org/10.1161/01.str.10.1.68>.
39. Meijer, O.C., de Lange, E.C., Breimer, D.D., de Boer, A.G., Workel, J.O., and de Kloet, E.R. (1998). Penetration of dexamethasone into brain glucocorticoid targets is enhanced in mdrlA P-glycoprotein knockout mice. *Endocrinology* *139*, 1789–1793. <https://doi.org/10.1210/endo.139.4.5917>.
40. Schinkel, A.H., Wagenaar, E., van Deemter, L., Mol, C.A., and Borst, P. (1995). Absence of the mdrlA P-Glycoprotein in mice affects tissue distribution and pharmacokinetics of dexamethasone, digoxin, and cyclosporin A. *J. Clin. Invest* *96*, 1698–1705. <https://doi.org/10.1172/JCI118214>.
41. Pardi, N., Tuyishime, S., Muramatsu, H., Kariko, K., Mui, B.L., Tam, Y.K., Madden, T.D., Hope, M.J., and Weissman, D. (2015). Expression kinetics of nucleoside-modified mRNA delivered in lipid nanoparticles to mice by various routes. *J. Control Release* *217*, 345–351. <https://doi.org/10.1016/j.jconrel.2015.08.007>.
42. Garcia, J.M., Stillings, S.A., Leclerc, J.L., Phillips, H., Edwards, N.J., Robicsek, S.A., Hoh, B.L., Blackburn, S., and Dore, S. (2017). Role of Interleukin-10 in Acute Brain Injuries. *Front Neurol.* *8*, 244. <https://doi.org/10.3389/fneur.2017.00244>.
43. Piepke, M., Clausen, B.H., Ludewig, P., Vienhues, J.H., Bedke, T., Javidi, E., Rissiek, B., Jank, L., Brockmann, L., Sandrock, I., et al. (2021). Interleukin-10 improves stroke outcome by controlling the detrimental Interleukin-17A response. *J. Neuroinflammation* *18*, 265. <https://doi.org/10.1186/s12974-021-02316-7>.
44. Kim, S.K., Keeney, S.E., Alpard, S.K., and Schmalstieg, F.C. (2003). Comparison of L-selectin and CD11b on neutrophils of adults and neonates during the first month of life. *Pediatr. Res.* *53*, 132–136. <https://doi.org/10.1203/00006450-200301000-00022>.
45. Ma, J., Ward, E.M., Siegel, R.L., and Jemal, A. (2015). Temporal Trends in Mortality in the United States, 1969–2013. *JAMA* *314*, 1731–1739. <https://doi.org/10.1001/jama.2015.12319>.
46. Lambertsen, K.L., Finsen, B., and Clausen, B.H. (2019). Post-stroke inflammation—target or tool for therapy? *Acta Neuropathol.* *137*, 693–714. <https://doi.org/10.1007/s00401-018-1930-z>.
47. Callegari, K., Dash, S., Uchida, H., Shingai, Y., Liu, C., Khodarkovskaya, A., Lee, Y., Ito, A., Lopez, A., Zhang, T., et al. (2023). Molecular profiling of the stroke-induced alterations in the cerebral microvasculature reveals promising therapeutic candidates. *Proc. Natl. Acad. Sci. USA* *120*, e2205786120. <https://doi.org/10.1073/pnas.2205786120>.
48. Jeon, S.B., Koh, Y., Choi, H.A., and Lee, K. (2014). Critical care for patients with massive ischemic stroke. *J. Stroke* *16*, 146–160. <https://doi.org/10.5853/jos.2014.16.3.146>.
49. Martin, M., Vermeiren, S., Bostaille, N., Eubelen, M., Spitzer, D., Vermeersch, M., Profaci, C.P., Pozuelo, E., Toussay, X., Raman-Nair, J., et al. (2022). Engineered Wnt ligands enable blood-brain barrier repair in neurological disorders. *Science* *375*, eabm4459. <https://doi.org/10.1126/science.abm4459>.
50. Posel, C., Moller, K., Boltze, J., Wagner, D.C., and Weise, G. (2016). Isolation and Flow Cytometric Analysis of Immune Cells from the Ischemic Mouse Brain. *J. Vis. Exp.* 53658. <https://doi.org/10.3791/53658>.
51. Kim, J.Y., Park, J., Chang, J.Y., Kim, S.H., and Lee, J.E. (2016). Inflammation after Ischemic Stroke: The Role of Leukocytes and Glial Cells. *Exp. Neurobiol.* *25*, 241–251. <https://doi.org/10.5607/en.2016.25.5.241>.
52. Gronberg, N.V., Johansen, F.F., Kristiansen, U., and Hasseldam, H. (2013). Leukocyte infiltration in experimental stroke. *J. Neuroinflammation* *10*, 115. <https://doi.org/10.1186/1742-2094-10-115>.
53. Uzdensky, A.B. (2019). Apoptosis regulation in the penumbra after ischemic stroke: expression of pro- and antiapoptotic proteins. *Apoptosis* *24*, 687–702. <https://doi.org/10.1007/s10495-019-01556-6>.
54. Schimmer, B.P., and Funder, J.W. (2017). Adrenocorticotropic Hormone, Adrenal Steroids, and the Adrenal Cortex. In *Goodman & Gilman's: The Pharmacological Basis of Therapeutics*, 13e, L.L. Brunton, R. Hilal-Dandan, and B.C. Knollmann, eds. (McGraw-Hill Education).
55. Norris, J.W. (2004). Steroids may have a role in stroke therapy. *Stroke* *35*, 228–229. <https://doi.org/10.1161/01.STR.0000105930.29558.DB>.
56. Pongvarin, N. (2004). Steroids have no role in stroke therapy. *Stroke* *35*, 229–230. <https://doi.org/10.1161/01.STR.0000105931.81723.26>.
57. Zhu, H., Hu, S., Li, Y., Sun, Y., Xiong, X., Hu, X., Chen, J., and Qiu, S. (2022). Interleukins and Ischemic Stroke. *Front Immunol.* *13*, 828447. <https://doi.org/10.3389/fimmu.2022.828447>.
58. Li, X., Lin, S., Chen, X., Huang, W., Li, Q., Zhang, H., Chen, X., Yang, S., Jin, K., and Shao, B. (2019). The Prognostic Value of Serum Cytokines in Patients with Acute Ischemic Stroke. *Aging Dis.* *10*, 544–556. <https://doi.org/10.14336/AD.2018.0820>.
59. Liang, Q.J., Jiang, M., Wang, X.H., Le, L.L., Xiang, M., Sun, N., Meng, D., and Chen, S.F. (2015). Pre-existing interleukin 10 in cerebral arteries attenuates subsequent

- brain injury caused by ischemia/reperfusion. *IUBMB Life* 67, 710–719. <https://doi.org/10.1002/iub.1429>.
60. Engel, O., Kolodziej, S., Dirnagl, U., and Prinz, V. (2011). Modeling stroke in mice - middle cerebral artery occlusion with the filament model. *J. Vis. Exp.* <https://doi.org/10.3791/2423>.
61. Hood, E.D., Greineder, C.F., Shuvaeva, T., Walsh, L., Villa, C.H., and Muzykantov, V.R. (2018). Vascular Targeting of Radiolabeled Liposomes with Bio-Orthogonally Conjugated Ligands: Single Chain Fragments Provide Higher Specificity than Antibodies. *Bioconjug. Chem.* 29, 3626–3637. <https://doi.org/10.1021/acs.bioconjchem.8b00564>.
62. Pardi, N., Muramatsu, H., Weissman, D., and Kariko, K. (2013). In vitro transcription of long RNA containing modified nucleosides. *Methods Mol. Biol.* 969, 29–42. https://doi.org/10.1007/978-1-62703-260-5_2.
63. Weissman, D., Pardi, N., Muramatsu, H., and Kariko, K. (2013). HPLC purification of in vitro transcribed long RNA. *Methods Mol. Biol.* 969, 43–54. https://doi.org/10.1007/978-1-62703-260-5_3.
64. Maier, M.A., Jayaraman, M., Matsuda, S., Liu, J., Barros, S., Querbes, W., Tam, Y.K., Ansell, S.M., Kumar, V., Qin, J., et al. (2013). Biodegradable lipids enabling rapidly eliminated lipid nanoparticles for systemic delivery of RNAi therapeutics. *Mol. Ther.* 21, 1570–1578. <https://doi.org/10.1038/mt.2013.124>.
65. Connors, J., Joyner, D., Mege, N., Cusimano, G., Bell, M., Marcy, J., Taramangalam, B., Lin, P., Tam, Y., Lin, P., et al. (2022). Lipid nanoparticles (LNP) induce activation and maturation of antigen presenting cells in young and aged individuals. *Res. Sq.* <https://doi.org/10.21203/rs.3.rs-2199652/v1>.
66. Parhiz, H., Brenner, J.S., Patel, P.N., Papp, T.E., Shahnawaz, H., Li, Q., Shi, R., Zamora, M.E., Yadegari, A., Marcos-Contreras, O.A., et al. (2022). Added to pre-existing inflammation, mRNA-lipid nanoparticles induce inflammation exacerbation (IE). *J. Control Release* 344, 50–61. <https://doi.org/10.1016/j.jconrel.2021.12.027>.